Michael Hörmannsdorfer, Ulrike Kahl and Tom Nilges*

Synthesis and characterization of Cu(II)-halide 1-methylimidazole complexes

DOI 10.1515/znb-2015-0139
Received August 25, 2015; accepted September 10, 2015

Abstract: Three new complexes of Cu(II) halides (Cl, Br) with 1-methylimidazole (MIm), $[Cu(MIm)_4]Br_2$ (**1**), $[Cu(MIm)_4Br]Br \cdot H_2O$ (**2**), and $[Cu(MIm)_6]Cl_2 \cdot 2H_2O$ (**3**) have been synthesized in ethanol. Their crystal structures have been determined by single-crystal X-ray diffraction. FT-IR spectroscopy, mass spectrometry, and thermal analyses were applied to characterize the compounds.

Keywords: crystal structures; divalent copper; 1-methylimidazole.

1 Introduction

Copper(II) halide methylimidazole complexes like $Cu(MIm)_2X_2$ and $[Cu(MIm)_4]X_2$ (X = Cl, Br) were studied by many groups in the last 60 years [1–4]. Complexes of the general formula $[Cu(MIm)_n]X_2$ (n = 1–5; X = Cl, Br) were investigated mainly for their catalytic behavior, e.g. for the oxidative carbonylation of methanol to dimethyl carbonate [5], as well as to act as a model system for the interactions between metal(II) ions and the imidazole derivate histidine in bio-systems [6, 7].

The structures of $Cu(MIm)_2Br_2$ [4], $Cu(MIm)_2Cl_2$ [8], and $[Cu(MIm)_2(H_2O)_2]Cl_2 \cdot H_2O$ [9] are known, and that of $[Cu(MIm)_4Br]Br \cdot H_2O$ is mentioned in Chinese patent CN 101498005 without giving any crystal structure data [10]. For complexes containing the cation $[Cu(MIm)_6]^{2+}$, no structures of halide salts are reported, but structures with other anions like tetraiodomercurate(II), salicylate, or bis(trifluoromethylsulfonyl) imide have been determined [11–14].

Herein we report on formation, structure determination, and characterization of three Cu(II) halide complexes with MIm.

2 Experimental section

All chemicals were commercially available and used without further purification.

2.1 Synthesis of $[Cu(C_4N_2H_6)_4]Br_2$ (1)

An excess of MIm (6 eq, 0.493 g, 6 mmol; Carl Roth) and 1 eq of $CuBr_2$ (0.223 g, 1 mmol; VWR) are dissolved in 10 mL of absolute ethanol (Prolabo, VWR), and the mixture is stirred at room temperature for 24 h. The resulting blue solution is concentrated by slow evaporation of ethanol in air, yielding deep blue plate-shaped crystals (0.502 g, 91 %). – Elemental analysis for $C_{16}H_{24}N_8CuBr_2$ (%): calcd. C 34.83, H 4.38, N 20.31; found C 34.57, H 4.39, N 19.87. – IR (ATR): ν = 3132, 3096, 3055, 2940, 2985, 1536, 1520, 1484, 1457, 1430, 1417, 1292, 1234, 1113, 1096, 1027, 948, 871, 847, 793, 754, 678, 664, 659, 624 cm^{-1}. – MS ((+)-FAB): *m/z* (%) = 137.2 (1.83), 145.2 (14.02) $[Cu(MIm)]^+$, 147.2 (6.12), 226.1 (1.17), 227.1 (100) $[Cu(MIm)_2]^{2+}$, 228.1 (10.01), 229.1 (41.66), 230.1 (4.16), 297.9 (1.31), 305.8 (10.28), 307.8 (11.98) $[Cu(MIm)Br]^+$, 308.9 (2.09), 309.8 (4.73), 368.7 (1.69), 370.7 (3.00), 372.7 (1.71), 387.8 (7.57), 388.8 (1.11), 389.7 (10.57) $[Cu(MIm)_3Br]^+$, 390.7 (1.52), 391.7 (3.41) 397.9 (1.03), 531.4 (1.10) $[Cu(MIm)_4Br]^+$, 533.4 (1.08).

2.2 Synthesis of $[Cu(C_4N_2H_6)_4Br]Br \cdot H_2O$ (2)

MIm (4 eq, 0.328 g, 4 mmol; Carl Roth) and $CuBr_2$ (1 eq, 0.223 g, 1 mmol, VWR) are dissolved in 10 mL of *absolute* ethanol (Prolabo, VWR) and stirred at r.t. for 24 h. The resulting blue solution is concentrated by slow evaporation of the ethanol in air, yielding deep blue plate shaped crystals. (0.527 g, 96 %). – Elemental analysis for $C_{16}H_{26}N_8O$-$CuBr_2$ (%): calcd. C 33.73, H 4.60, N 19.67; found C 34.46, H 4.38, N 19.79. – IR (ATR): ν = 3547 (O–H), 3420, 3375, 3249,

***Corresponding author: Tom Nilges,** Department of Chemistry, Technische Universität München, Lichtenbergstrasse 4, D-85747 Garching, Germany, Fax: +49-89-289-13186, E-mail: tom.nilges@lrz.tu-muenchen.de
Michael Hörmannsdorfer and Ulrike Kahl: Department of Chemistry, Technische Universität München, Lichtenbergstrasse 4, D-85747 Garching, Germany

3105, 3053, 2998, 2985, 2956, 2940, 2896, 2864, 2825, 2769, 2745, 2662, 2626, 2578, 1732, 1701, 1636, 1607, 1583, 1534, 1519, 1456, 1417, 1376, 1343, 1286, 1233, 1171, 1099, 1027, 949, 870, 843, 828, 789, 755, 664, 621, 572, 475 cm^{-1}. – MS ((+)-FAB): *m/z* (%) = 137.2 (2.31), 145.2 (14.94) $[Cu(MIm)]^+$, 147.2 (6.33), 226.1 (1.34), 227.1 (100) $[Cu(MIm)_2]^+$, 228.1 (9.62), 229.1 (40.75), 230.1 (4.12), 297.9 (1.59), 305.8 (9.75), 307.8 (12.16) $[Cu(MIm)_2Br]^+$, 308.9 (2.12), 309.8 (4.38), 368.7 (1.35), 370.6 (2.35) $[Cu(MIm)_2Br]^+$, 372.6 (1.30), 387.8 (7.76), 388.7 (1.22), 389.7 (11.11) $[Cu(MIm)_3Br]^+$, 390.7 (1.69), 391.7 (3.50) 397.9 (2.40), 399.9 (1.15), 533.3 (1.05).

2.3 Synthesis of $[Cu(C_4N_2H_6)_6]Cl_2 \cdot 2H_2O$ (3)

MIm (4 eq, 0.328 g, 4 mmol, Carl Roth) and $CuCl_2 \cdot 2H_2O$ (1 eq, 0.153 g, 1 mmol) are dissolved in 10 mL of absolute ethanol (Prolabo, VWR) and stirred at r.t. for 24 h. The resulting blue solution is concentrated by slow evaporation of the ethanol at air, yielding blue crystals. (0.597 g, 90 %). – Elemental analysis for $C_{16}H_{28}N_8O_2CuCl_2$ (%): calcd. C 43.47, H 6.08, N 25,35; found C 43.18, H 6.04, N 24.92. – IR (ATR): *v* = 3459 (O–H), 3395, 3143, 3251, 3112, 3092, 1623, 1533, 1422, 1284, 1244, 1101, 1081, 1027, 947, 917, 862, 833, 761, 659, 620, 573, 532 cm^{-1}. – MS ((+)-FAB): *m/z* (%) = 137.2 (2.73), 145.2 (22.18) $[Cu(MIm)]^+$, 147.2 (9.03), 226.1 (1.36), 227.1 (100) $[Cu(MIm)_2]^+$, 228.1 (10.22), 229.1 (42.09), 230.1 (3.95), 262.0 (36.89), 263.0 (4.86), 264.0 (28.91) $[Cu(MIm)_2Cl]^+$, 265.0 (3.37), 266.0 (5.55), 297.9 (1.23), 324.8 (1.85), 326.8 (2.39), 343.9 (15.77), 344.9 (2.32), 345.9 (12.46) $[Cu(MIm)_3Cl]^+$, 346.9 (1.75), 347.9 (2.21), 397.9 (2.54), 399.9 (1.11).

2.4 X-ray structure determinations

Single-crystal data were collected on an Oxford XCalibur3 (for **1** and **3**) and a Bruker APEX-II CCD (for **2**) with graphite-monochromatized MoK_α radiation (λ = 0.71073 Å). The sample crystals were cooled by nitrogen flow to 120 K. The structures were solved using the software package JANA2006 [15, 16]. All non-hydrogen atoms were refined anisotropically, whereas the hydrogen atoms were restricted to 1.2 times of the ADP value of the neighboring carbon atoms and were refined isotropically. Table 1 contains the crystal data and numbers pertinent to data collection and structure refinement, and Table 2 summarizes important distances and angles. Atomic coordinates and isotropic and equivalent isotropic displacement parameters

Table 1: Crystal structure data for $[Cu(MIm)_4]Br_2$ (**1**), $[Cu(MIm)_4Br]Br \cdot H_2O$ (**2**), and $[Cu(MIm)_6]Cl_2 \cdot 2H_2O$ (**3**).

	1	**2**	**3**
Formula	$C_{16}H_{24}N_8Br_2Cu$	$C_{16}H_{26}N_8OBr_2Cu$	$C_{24}H_{40}N_{12}O_2Cl_2Cu$
M_r	551.8	569.8	663.1
Crystal size, mm^3	0.33 × 0.09 × 0.20	0.27 × 0.21 × 0.12	0.23 × 0.30 × 0.19
Crystal system	monoclinic	triclinic	monoclinic
Space group	$P2_1/c$ (no. 14)	$P\bar{1}$ (no. 2)	$P2_1/c$ (no. 14)
a, Å	7.4865(2)	9.1966(4)	8.2020(2)
b, Å	9.3235(3)	9.7266(4)	13.3448(5)
c, Å	16.4178(5)	13.364(5)	15.3572(5)
α, deg	90	88.157(2)	90
β, deg	115.798(3)	80.967(2)	112.661(2)
γ, deg	90	78.465(2)	90
V, $Å^3$	1031.75(6)	1128.41(8)	1551.14(9)
Z	2	2	2
D_{calcd}, g cm^{-3}	1.78	1.68	1.42
μ(MoK_α), cm^{-1}	49.5	45.3	9.2
F(000), e	550	570	694
hkl range	−10→+11, ±14, ±25	±13, ±14, ±19	±12, −19→+20, ±23
$((\sin\theta)/\lambda)_{max}$, $Å^{-1}$	0.780	0.751	0.779
Reflections, measured	19899	52511	30300
Reflections, unique/R_{int}	3789/0.038	5681/0.054	5353/0.059
Parameter refined	125	254	188
$R(F)/wR(F^2)$[a] (all reflection)	0.025/0.059	0.031/0.104	0.037/0.086
GoF (F^2)[a]	0.0125	0.0226	0.0147
$\Delta\rho_{fin}$ (max/min), e $Å^{-3}$	0.47/−0.36	0.75/−0.53	0.40/−0.41

[a] $w = 1/(\sigma^2(I) + 0.0004I^2)$.

Table 2: Selected bond angles (deg) and bond lengths (Å) for $[Cu(MIm)_4]Br_2$ (**1**), $[Cu(MIm)_4Br]Br \cdot H_2O$ (**2**), and $[Cu(MIm)_6]Cl_2 \cdot 2H_2O$ (**3**).

$[Cu(MIm)_4]Br_2$ (**1**)			
Cu1–N23	1.999(1)	Br1–Cu1–N13	90.6(1)
Cu1–N13	2.012(2)	Br1–Cu1–N23	90.8(1)
Cu1–Br1	3.257(1)	N13–Cu1–N23	89.0(1)
$[Cu(MIm)_4Br]Br \cdot H_2O$ (**2**)			
Cu1–N43	1.997(3)	N13–Cu1–N23	90.6(1)
Cu1–N13	2.006(3)	N13–Cu1–N43	90.8(1)
Cu1–N23	2.018(3)	N23–Cu1–N33	88.5(1)
Cu1–N33	2.022(3)	N43–Cu1–N33	87.8(1)
Cu1–Br1	2.778(1)	N13–Cu1–N33	167.4(1)
Cu1–Br2	3.810(1)	N23–Cu1–N43	169.2(1)
		Br1–Cu1–N13	96.4(1)
		Br1–Cu1–N23	94.6(1)
		Br1–Cu1–N33	96.2(1)
		Br1–Cu1–N43	95.9(1)
$[Cu(MIm)_6]Cl_2 \cdot 2H_2O$ (**3**)			
Cu1–N23	2.025(1)	N13–Cu1–N23	91.4(1)
Cu1–N13	2.040(1)	N13–Cu1–N33	90.2(1)
Cu1–N33	2.537(1)	N23–Cu1–N33	94.1(1)

for the structure determinations are available online as Supporting Information (see note at the end of the paper for availability).

CCDC 1403820 ($[Cu(MIm)_4]Br_2$, **1**), 1403821 ($[Cu(MIm)_4Br]Br \cdot H_2O$, **2**), and 1403822 ($[Cu(MIm)_6]Cl_2 \cdot 2H_2O$, **3**) contain the supplementary crystallographic data for this paper. These data can be obtained free of charge from the Cambridge Crystallographic Data Centre *via* www.ccdc.cam.ac.uk/data_request/cif.

2.5 Thermal analysis

Differential scanning calorimetry (DSC) was performed with a DSC 200 F3 Maia from Netzsch applying a heating rate of 10 K min^{-1}. Each sample, 11–15 mg, was filled in aluminum pans and measured against an empty crucible. Data handling was executed with the program PROTEUS Thermal Analysis [17].

Thermal gravimetric analysis (TGA) was performed with a TGA/DSC 1 from Mettler Toledo in an argon atmosphere with a heating rate of 10 K min^{-1}. For each analysis, 3 mg of sample was used.

2.6 IR spectroscopy and mass spectrometry

IR spectra were obtained on a Spectrum Two FT-IR Spectrometer (Typ UATR Two; Perkin Elmer).

FAB mass spectra were collected with a MAT 90 (Finnigan MAT) in positive mode using a 1-nitrobenzyl chloride matrix. The main peak in all three compounds appeared at $m/z = 227$ and was assigned to $[Cu(MIm)_2]^+$.

3 Results and discussion

3.1 Synthesis procedures

Syntheses of the title compounds **1**–**3** were attempted in ethanol as solvents. For the synthesis of **1** and **2**, the same educts were used with different amounts of MIm. In case of **1**, a 1:6 ratio of $CuBr_2$ to MIm was used, resulting in the water-free complex, whereas in the case of **2**, only 4 eq of MIm was reacted, yielding the monohydrate complex. Both results are reproducible. As all reaction parameters were kept identical except the amount of the MIm ligand, the formation of the monohydrate complex is somewhat unexpected. The solvent itself and $CuBr_2$ as the origin of water is negligible because absolute ethanol and the same $CuBr_2$ were used for both syntheses. Obviously, the reason of gaining water-free $[Cu(C_4N_2H_6)_4]Br_2$ is connected with the concentration of the ligand MIm in the reaction mixture. As MIm evaporates slower than ethanol, a small amount of the ligand might stay on the surface of the grown crystals protecting them against moisture. In good agreement with this assumption, we observed that **1** tends to absorb water over a period of several weeks, resulting in **2**.

3.2 Solid-state structures

All single crystals were deep blue in color and showed plate-like morphology. A summary of crystal structure data is given in Table 1.

$[Cu(MIm)_4]Br_2$ (**1**) crystallizes in the monoclinic space group $P2_1/c$ with $Z = 2$. The complex is shown in Fig. 1. Cu1 is octahedrally coordinated by four MIm ligands and two bromide anions. A square-planar arrangement of four MIm ligands in equatorial position was found, with the remaining two bromide anions occupying axial positions. Owing to the overall symmetry, the octahedron around Cu1 contains two crystallographically independent MIm ligands and one Br^- anion. Going clockwise from ligand to ligand, the MIm rings are twisted by 90 deg around the Cu–N bond. Distances between Cu1 and N13 and between Cu1 and N23 are 1.999(1) and 2.012(2) Å, respectively. Such bond lengths are comparable with the ones found in complexes like $Cu(NH_3)_4(NO_3)_2$ and $[Cu(MIm)_4(H_2O)_2]Cl_2 \cdot H_2O$

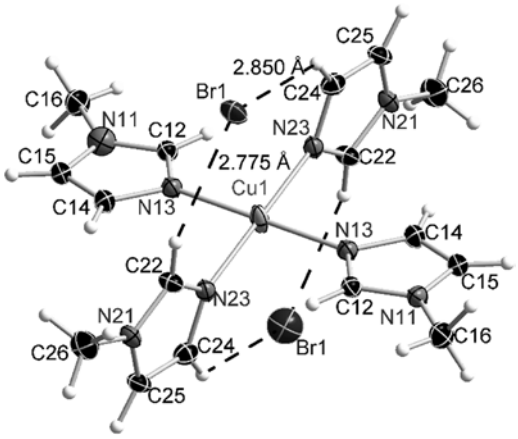

Fig.1: Molecular structure of $[Cu(MIm)_4]Br_2$ (**1**) in the crystal with atom numbering adopted. Displacement ellipsoids for Cu, Br, C, and N are drawn at the 50 % probability level.

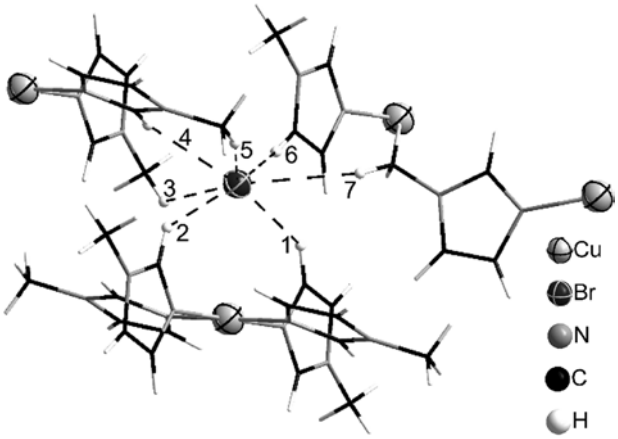

Fig. 3: H bond network among four complex units in crystals of $[Cu(MIm)_4]Br_2$ (**1**). H···Br bonds are numbered (with distances in Å): 1 = 2.850(1), 2 = 2.775(1), 3 = 3.131(1), 4 = 2.945(1), 5 = 2.883(1), 6 = 2.950(1), and 7 = 3.007(1).

[9, 18]. The axial Cu–Br bond distance is 3.257(1) Å and thus significantly longer than in $CuBr_2$ (2.414 Å) [19]. Therefore, the interaction between Cu(1) and Br(1) is rather weak. All bond distances and angles of interest are listed in Table 2.

Cu is located at each corner of the unit cell and at the center of the [011] plane. $[Cu(MIm)_4]^{2+}$ units and Br^- are stacked along the crystallographic *a* axis (see Fig. 2).

The interaction between different complex molecules is realized by hydrogen bonds with bromide as acceptor (see Fig. 3). The hydrogen bond network among four complex units is shown in Fig. 3: 1 = 2.850(1), 2 = 2.775(1), 3 = 3.131(1), 4 = 2.945(1), 5 = 2.883(1), 6 = 2.950(1), and 7 = 3.007(1) Å). Br^- ions form seven different hydrogen bonds in the range of 2.775(1)–3.131(1) Å, of which no. 1 and 2 are representative intramolecular bonds with the shortest donor–acceptor distances. Those interactions are the reason for the widened Cu–Br distance, as was observed by Clegg et al. [9] for the axial aqua ligands in $[Cu(MIm)_4(H_2O)_2]Cl_2 \cdot H_2O$. Five hydrogen bonds (no. 3–7) connect Br1 to three neighboring complexes, whereas no. 5–7 are within the same complex molecule. All donor–acceptor interactions are classified as weak [20].

$[Cu(MIm)_4Br]Br \cdot H_2O$ (**2**) crystallizes in the triclinic space group $P\bar{1}$ with $Z = 2$. Compared with **1**, the additional water molecule lowers the symmetry from monoclinic to triclinic. The cell volume expands from 1031.75(6) to 1128.41(8) Å^3. In Fig. 4, the molecular structure is shown.

The coordination geometry of the Cu atom is a tetragonal pyramid with four equatorial MIm ligands and Br1 in

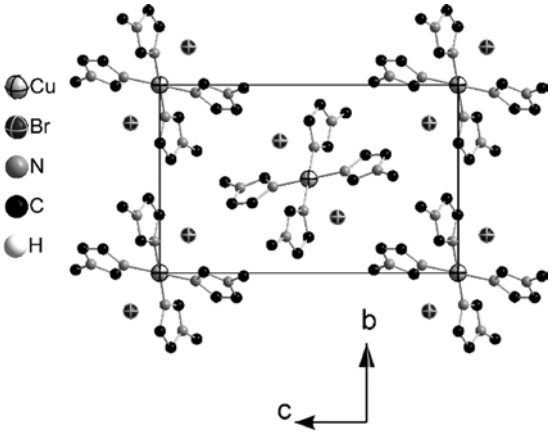

Fig. 2: Unit cell of $[Cu(MIm)_4]Br_2$ (**1**) as viewed along the crystallographic *a* axis. H atoms are omitted for clarity.

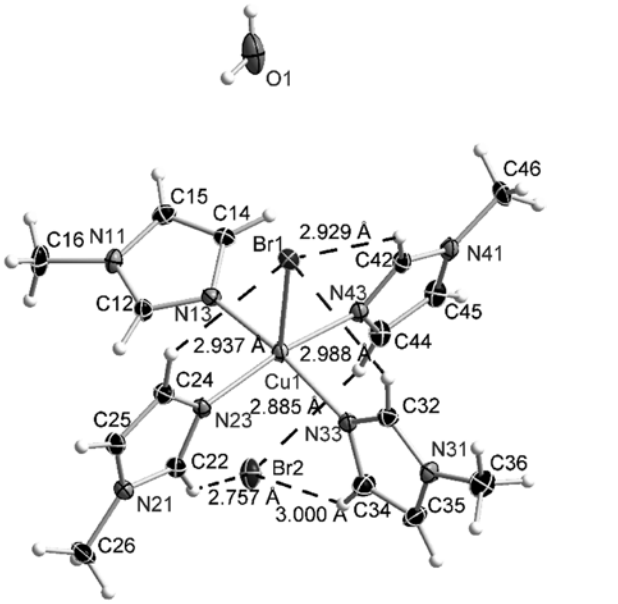

Fig. 4: Molecular structure of $[Cu(MIm)_4Br]Br \cdot H_2O$ (**2**) in the crystal with atom numbering adopted. Displacement ellipsoids for Cu, Br, C, and N are drawn at the 50 % probability level.

the axial position. The angles N13–Cu1–N33 of 167.4(1)° and N23–Cu1–N43 of 169.2(1)° indicate that Cu1 is located slightly above the plane spanned by MIm ligands. Br2 is an outer complex ligand and located slightly aside of the hypothetical Cu1–Br1 axis. The imidazole rings are rotated relative to the opposite ligands: ring 1 stands perpendicular to ring 3, and ring 2 is turned by 180° relative to ring 4. The Cu–N bond distances range between 1.997(3) Å (Cu1–N43) and 2.018(3) Å (Cu1–N23), which is comparable to literature values found in $Cu(NH_3)(NO_3)_2$ and $[Cu(MIm)_4(H_2O)_2]Cl_2 \cdot H_2O$ [9, 18]. The Cu1–Br1 bond length in **2** is 2.778(4) Å, which is longer than the $CuBr_2$ bond length (2.414 Å) [19]. A much longer distance of 3.810(5) Å has been determined for Cu1–Br2. Therefore, it must be assumed that the dominant interaction between these two atoms is electrostatic in nature. All interesting bond distances and angles are listed in Table 2. In Fig. 5, the stacking along the *a* axis can be seen.

The crystal structure is determined by a complex hydrogen bond system among water molecules, H atoms of the MIm ligand, and Br^- anions (see Fig. 6). With distances 2.757(1)–3.336(1) Å, Br1 forms 8 (no. 1–8) and Br2 form 10 hydrogen bonds (no. 9–18). Br1 interacts with water (no. 7) at a distance of 3.193(1) Å and Br2 with both hydrogen of the H_2O unit (no. 15 and 16) at distances of 2.828(1) and 3.336(1) Å, respectively. No. 1–4 are intramolecular bonds to Br1, whereas no. 5–8 connect the complex molecule to three neighbors. Br2 is only attached to the complex by hydrogen bonds. This is realized *via* bonds no. 9, 11, and 12. Furthermore, Br2 is bound to five neighbors (no. 10 and 13–18). The H bonds are classified as weak [20].

$[Cu(MIm)_6]Cl_2 \cdot 2H_2O$ (**3**) crystallizes in the monoclinic space group $P2_1/c$ with $Z = 2$. The molecular structure is shown in Fig. 7. Six MIm ligands coordinate octahedrally to Cu. In the centrosymmetric complex, three crystallographically different MIm units are realized.

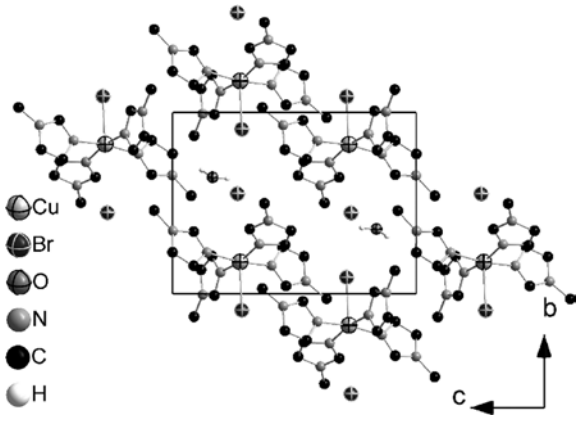

Fig. 5: Unit cell of $[Cu(MIm)_4Br]Br \cdot H_2O$ (**2**) as viewed along the crystallographic *a* axis. H atoms are omitted for clarity.

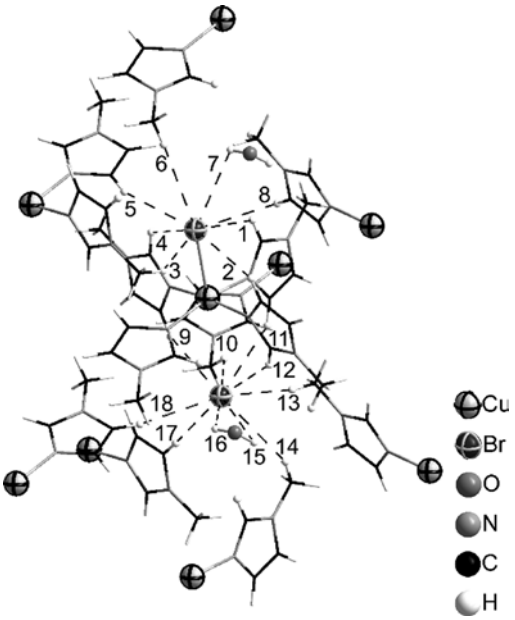

Fig.6: H bond network among four complexes in crystals of $[Cu(MIm)_4Br]Br \cdot H_2O$ (**2**). The H···Br bonds are numbered (with distances in Å): 1 = 2.988(1), 2 = 2.937(1), 3 = 2.881(1), 4 = 2.929(1), 5 = 2.899(1), 6 = 3.328(1), 7 = 3.193(1), 8 = 3.189(1), 9 = 2.885(1), 10 = 3.232(1), 11 = 3.000(1), 12 = 2.757(1), 13 = 3.118(1), 14 = 3.185(1), 15 = 3.336(1), 16 = 2.828(1), 17 = 2.773(1), and 18 = 3.259(1).

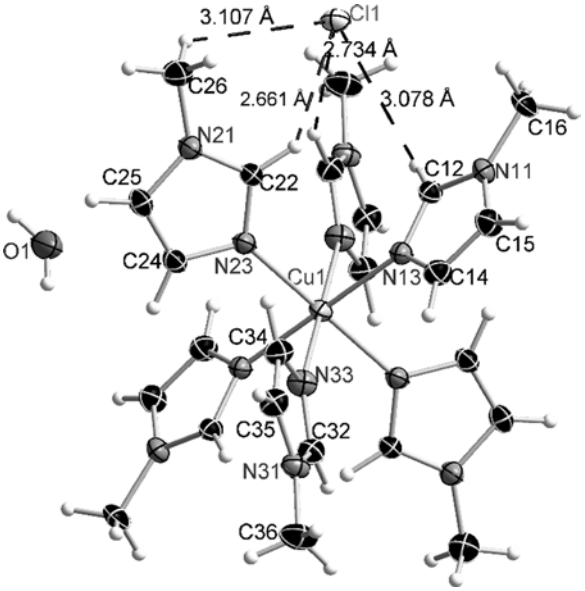

Fig. 7: Molecular structure of $[Cu(MIm)_6]Cl_2 \cdot 2H_2O$ (**3**) in the crystal with atom numbering adopted. Displacement ellipsoids for Cu, Br, C, N, and O are drawn at the 50 % probability level.

Similar to **1**, the rings in the basal plane are turned by 90° around the Cu–N bond, going clockwise from ligand to ligand, to minimize the steric interactions between the methyl groups. The Cu–N bond lengths in the complex

vary between 2.025(1) Å (Cu–N23) and 2.040(2) Å (Cu–N13) for the basal and 2.537(2) Å for the axial ligands (Cu–N33), showing a slight Jahn-Teller distortion from the octahedral geometry. All interesting bond distances and angles are listed in Table 2. The geometry and distances are quite similar to those of hexakis(imidazole)copper(II) diaspirinate described by Abuhijleh et al. [12] in 2001. Chloride ions are outer complex ligands and do not coordinate to the central Cu(II) ion, which is sterically shielded by six MIm ligands.

In the unit cell, Cu is located at the corners and the center (see Fig. 8).

Molecules of (**3**) are stacked along the crystallographic *b* axis. The complex molecules are connected to each other *via* hydrogen bonds (see Fig. 9). Cl1 builds four intramolecular bonds (no. 1–4) at distances of 1 = 3.078(1), 2 = 2.661(1), 3 = 2.734(1), and 4 = 3.107(1) Å. In addition, Cl1 is attached to a network of four neighbors (no. 5, 7–9, 11) and both hydrate molecules (no. 6 and 10) at distances of 3.375(1)–3.107(1) Å. H bonds to water molecules connect the anions. All H bonds in this compound are classified to be weak [20].

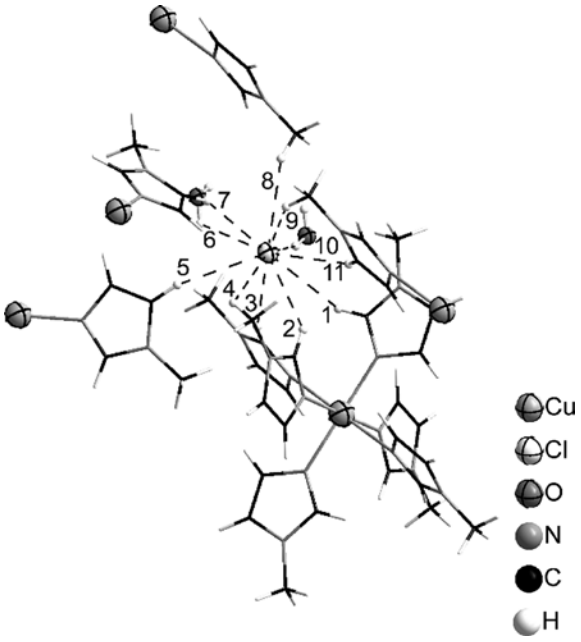

Fig. 9: H bond network among four complex units in crystals of $[Cu(MIm)_6]Cl_2 \cdot 2H_2O$ (**3**). The H···Cl bonds are numbered (with distances in Å): 1 = 3.078(1), 2 = 2.661(1), 3 = 2.734(1), 4 = 3.107(1), 5 = 2.878(1), 6 = 2.685(1), 7 = 2.697(1), 8 = 2.887(1), 9 = 2.965(1), 10 = 2.375(1), and 11 = 2.924(1) Å.

3.3 Thermal analysis

Compounds **1**–**3** were subjected to thermal analysis to evaluate the stability and behavior of the phases. The DSC plot (Fig. 10) of **1** shows one non-reversible effect with an onset value of 450 K for decomposition in a one-step reaction.

In contrast, two thermal effects are present in the DSC plot of **2**, at 390 and 435 K. A TGA plot (Fig. 11) of **2** shows only one thermal effect, which matches with the second effect in the DSC measurement. Therefore, the first DSC

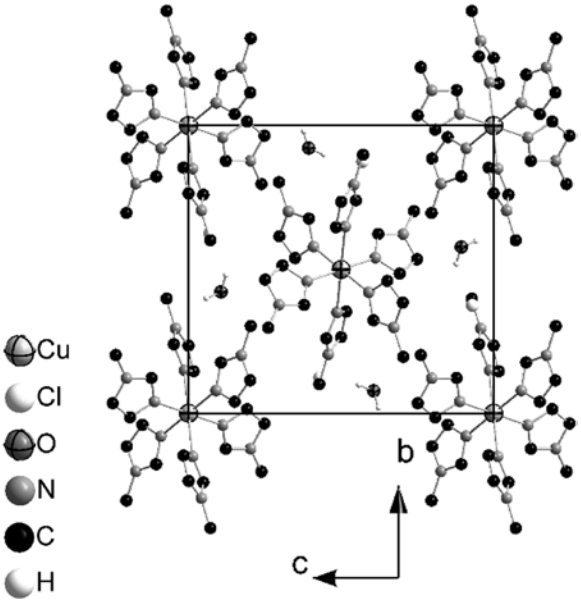

Fig. 8: Unit cell of $[Cu(MIm)_6]Cl_2 \cdot 2H_2O$ (**3**) as viewed along the crystallographic *a* axis. H atoms are omitted for clarity.

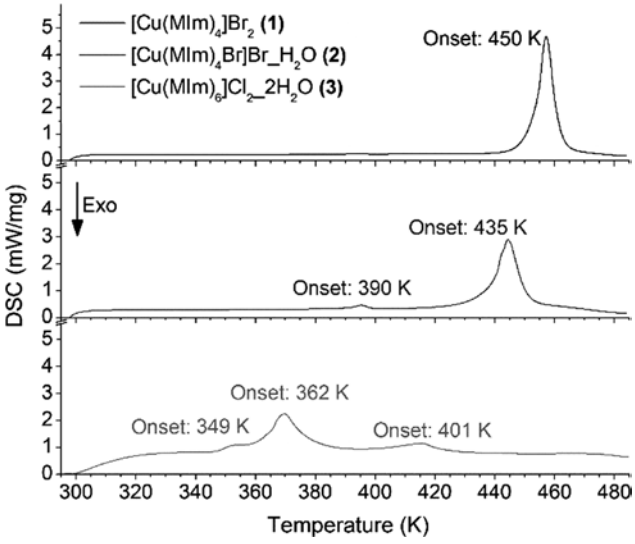

Fig. 10: DSC analyses of **1**, **2**, and **3** in the temperature range of 298 to 493 K with a heating rate of 10 K min^{-1}.

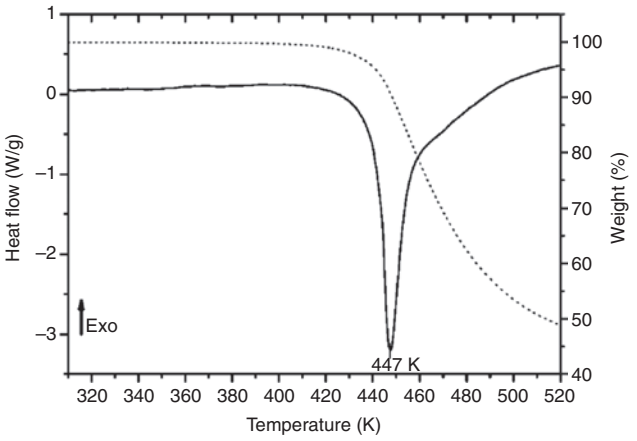

Fig. 11: TGA of $[Cu(MIm)_4Br]Br \cdot H_2O$ (**2**). The dotted line represents the weight reduction; solid line, heat flow.

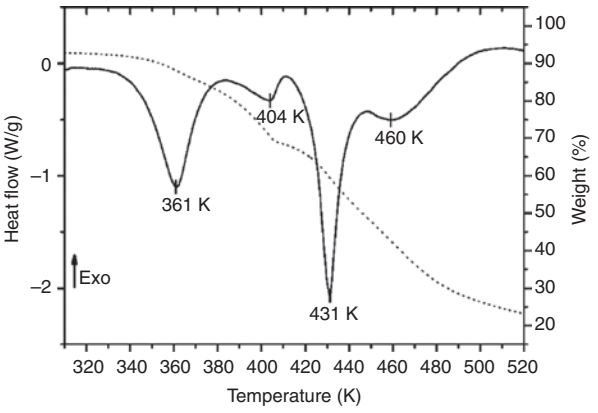

Fig. 12: TGA of $[Cu(MIm)_6]Cl_2 \cdot 2H_2O$ (**3**). The dotted line represents the weight reduction, the solid line the heat flow.

effect is attributed to an intramolecular rearrangement, as no weight reduction was detected. The decomposition of **2** starts at 435 K, with its maximum at 447 K. This is a one-step reaction like with **1**, which indicates that the hydrate molecule destabilizes the structure. The residues of both **1** and **2** were analyzed by powder XRD after the DSC measurement but could not be identified.

In the work of van Berkum et al. [3], a thermal analysis of $[Cu(MIm)_4]Br_2$ (**1**) was also performed. In contrast to our measurements, they observed three effects that they assigned to two decompositions from 353 to 423 and from 436 to 569 K and a melting point at 432 K. In the first thermal effect, Berkum et al. postulate the release of two equivalents of MIm and the intermediate formation of $[Cu(MIm)_2Br_2]$. The two decomposition steps match with our measurements. As **1** was observed to absorb water over a couple of weeks, we think that van Berkum et al. unintentionally used compound **2** for their measurements.

The DSC plot of **3** shows three endothermic irreversible effects at 349, 362, and 401 K, which suggests a three-step decomposition. In contrast, the TGA (Fig. 12) plot shows four effects with maxima at 361, 404, 431, and 459 K. The first effect of the DSC measurement was not detected in the TGA experiment. This could derive from the fact that a much lower amount of compound was used for the TGA, and so the weak first effect from the DSC is an element of the following broad peak. This effect and the next one are present in both measurements. Following are two effects with maxima at 431 and 459 K, which only appear in the TGA. This originates from the two different measurement types, as the same batch was used for both analyses. DSC was done in a closed aluminum container; the crucible for the TGA was open. The weight reduction at the first step at 361 K is equal to the release of 2 eq of water and 1 eq of MIm from **3**; the second effect at 404 K represents a reduction by further 2 eq of MIm. In the following, 1 eq of MIm gets lost at 431 and 459 K. At the end of the measurement, 24.1 % of the original weight is left, which comes up to a sum formula of the residue equal to $CuCl_2$ and 1 eq of MIm. The residue was analyzed by powder XRD but could not be identified.

4 Conclusion

MIm and Cu(II)X_2 (X = Cl, Br) can be reacted to organometallic complexes in ethanol. Structures of monoclinic $[Cu(MIm]_4]Br$ (space group $P2_1/c$), triclinic $[Cu(MIm)_4Br]Br \cdot H_2O$ (space group $P\bar{1}$), and monoclinic $[Cu(MIm)_6]Cl_2 \cdot 2H_2O$ (space group $P2_1/c$) were determined by single crystal X-ray diffraction. The compounds were characterized by FT-IR spectroscopy and mass spectrometry. Through DSC and TGA, we identified the decomposition points of $[Cu(MIm]_4]Br_2$ (**1**), $[Cu(MIm)_4Br]Br \cdot H_2O$ (**2**), and $[Cu(MIm)_6]Cl_2 \cdot 2H_2O$ (**3**). We have shown with the aid of thermal analysis and structure data that water-free $[Cu(MIm]_4]Br_2$ as described earlier in the literature might contained water as in our $[Cu(MIm)_4Br]Br \cdot H_2O$ (**2**).

Based on the structural chemistry reported in this paper, we hope that this set of compounds will act as additional model systems for histidine in biological systems and that their catalytic behavior will be tested.

Supporting information: Atomic coordinates and isotropic and equivalent isotropic displacement parameters for $[Cu(MIm)_4]Br_2$ (**1**), $[Cu(MIm)_4Br]Br \cdot H_2O$ (**2**), and $[Cu(MIm)_6]Cl_2 \cdot 2H_2O$ (**3**) are given as Supporting Information (DOI: 10.1515/znb-2015-0139).

Acknowledgments: We thank Carolin Grotz for the DSC measurements, Rodica Dumitrescu for the mass spectrometry, and Prof. Dr. Hubert Gasteiger for permission to use the IR spectrometer and TGA. Funding from the TUM Graduate School for this work is gratefully acknowledged.

References

[1] D. Goodgame, M. Goodgame, G. W. Rayner-Canham, *Inorg. Chim. Acta* **1969**, *3*, 406.
[2] J. A. Welleman, F. B. Hulsbergen, J. Verbiest, J. Reedijk, *J. Inorg. Nucl. Chem.* **1978**, *40*, 143.
[3] J. G. van Berkum, G. Hakvoort, J. Reedijk, *Thermochim. Acta* **1981**, *43*, 49.
[4] J. C. Jansen, H. van Konigsveld, J. A. C. van Ooijen, *Cryst. Struct. Commun.* **1978**, *7*, 637.
[5] V. Raab, M. Merz, J. Sundermeyer, *J. Mol. Catal. A* **2001**, *175*, 51.
[6] L. E. Cheruzel, M. R. Cecil, S. E. Edison, M. S. Mashuta, M. J. Baldwin, R. M. Buchanan, *Inorg. Chem.* **2006**, *45*, 3191.
[7] R. Gillard, *Inorg. Chim. Acta Rev.* **1967**, *1*, 69.
[8] J. A. C. van Ooijen, J. Reedijk, A. L. Spek, *J. Chem. Soc. Dalton Trans.* **1979**, 1183.
[9] W. Clegg, J. R. Nicholson, D. Collison, C. D. Garner, *Acta Crystallogr.* **1988**, *C44*, 453.
[10] Y. Yaxian, Y. Jianlin, CN101498005 (A), **2009**.
[11] L. Gao, *Russ. J. Coord. Chem.* **2014**, *40*, 138.
[12] A. L. Abuhijleh, C. Woods, *Inorg. Chem. Commun.* **2001**, *4*, 119.
[13] T. Vander Hoogerstraete, N. R. Brooks, B. Norberg, J. Wouters, K. van Hecke, L. van Meervelt, K. Binnemans, *CrystEngComm.* **2012**, *14*, 4902.
[14] Y.-K. Lv, Z.-G. Jiang, J. Chen, X. J. Wanf, Y.-L. Feng, *J. Inorg. Organomet. Polym. Mater.* **2011**, *21*, 223.
[15] V. Petříček, M. Dušek, L. Palatinus, JANA2006, The Crystallographic Computing System, Institute of Physics, Academy of Sciences of the Czech Republic, Prague (Czech Republic) **2006**.
[16] V. Petříček, M. Dušek, L. Palatinus, *Z. Kristallogr. Cryst. Mater.* **2014**, *229*, 345.
[17] PROTEUS (version 5.2.0), Netzsch, Selb, Germany **2010**.
[18] B. Morosin, *Acta Crystallogr.* **1976**, *B32*, 1237.
[19] O. Oeckler, A. Simon, *Z. Kristallogr. NCS* **2000**, *215*, 13.
[20] T. Steiner, *Angew. Chem. Int. Ed.* **2002**, *41*, 48.

Supplemental Material: The online version of this article (DOI:10.1515/znb-2015-0139) offers supplementary material, available to authorized users.